Revisiting the Butler-Mokrys Model for the Vapor-Extraction Process

V. Mohan, P. Neogi, and **B. Bai,** Missouri University of Science and Technology

Summary

The dynamics of a process in which a solvent in the form of a vapor or gas is introduced in a heavy-oil reservoir is considered. The process is called the solvent vapor-extraction process (VAPEX). When the vapor dissolves in the oil, it reduces its viscosity, allowing oil to flow under gravity and be collected at the bottom producer well. The conservation-of-species equation is analyzed to obtain a more-appropriate equation that differentiates between the velocity within the oil and the velocity at the interface, which can be solved to obtain a concentration profile of the solvent in oil. We diverge from an earlier model in which the concentration profile is assumed. However, the final result provides the rate at which oil is collected, which agrees with the previous model in that it is proportional to $\sqrt{h}$, where h is the pay-zone height; in contrast, some of the later data show a dependence on h. Improved velocity profiles can capture this dependence. A dramatic increase in output is seen if the oil viscosity decreases in the presence of the solvent, although the penetration of the solvent into the oil is reduced because under such conditions the diffusivity decreases with decreased solvent. One other important feature we observe is that when the viscosity-reducing effect is very large, the recovered fluid is mainly solvent. Apparently, some optimum might exist in the solubility φ_o, where the ratio of oil recovered to solvent lost is the largest. Finally, the present approach also allows us to show how the oil/vapor interface evolves with time.

Introduction

Heavy crude has a very high viscosity, making it difficult to extract the crude from underground reservoirs. One method used to decrease the viscosity is using steam to heat up the oil when the oil viscosity drops to a value such as 1 cp and drains out under gravity to 5 to 10 cp at the producer well. This method is termed steam-assisted gravity drainage. In another process, a solvent in vapor form is used, and dissolution of the vapor into oil lowers the viscosity. This is the solvent VAPEX process (Banerjee 2012). The solvent used can be vapors of C_7 and lower hydrocarbons. If the gas is carbon dioxide (CO_2), the process can be used for CO_2 sequestration. Some oil that is recovered can be used to pay for the process, provided that not too much CO_2 is lost alongside (Shaw and Bachu 2002; Bachu and Shaw 2003). Aghbash and Ahmadi (2012) show good comparison between simulation and laboratory results with a system that matches field permeability and its variation with depth. Some have added steam to improve the recovery part of the process (Naderi and Babadagli 2012). Kok and Ors (2012) present simulation studies to widen the scope of an ongoing process. These types of studies continue to be seen because sequestration is usually the last stage (Jia et al. 2017; Temizel et al. 2017).

The VAPEX process uses two horizontal wells. The top well is the injection well, and the bottom well picks up the drainage. Butler and Mokrys (1989) were the first to quantify oil recovery, and we have reworked that process here. They used a vertically held Hele-Shaw cell, introduced the vapor from the side, and collected the drainage at the bottom corner. From the rate of collection, they were able to verify that the dependence on reservoir height and permeability from their model was correct. The fact that some hydrocarbons precipitate asphaltenes has been long known (Burke et al. 1990), and an organized view of precipitation thermodynamics also exists (Nghiem and Coombe 1997). From a practical point of view, the precipitate can plug the wellbore region, and discourses on what to do to relieve it also exist (Haghighat and Maini 2012a).

In the following, we review the Butler and Mokrys (1989) approach, with an emphasis on how the boundary-value problem should be set up and what the new solution is like. Approximately 15% of the oil is expected to be lost as precipitate, and some thoughts regarding how asphaltene precipitation can be worked into the model are required. Further, the existing approach does not locate the interface or its changes with time.

Transport Model and Order-of-Magnitude Analysis

The basic setup is shown in **Fig. 1.** If CO_2 is introduced as the solvent, then under reservoir conditions CO_2 can be a gas or a liquid. However, some experiments show that even at 5,000 psi, miscibility of CO_2 and heavy crude is not reached (Chung et al. 1988). With methane as a solvent, it would not liquefy under reservoir conditions. Consequently, for these two solvents, the boundary condition at the solvent/oil interface on the oil side is that the volume fraction of the solvent there is φ_o, a quantity dependent on the pressure in the solvent-phase P. The pressure P can be taken to be a constant because the dissolution process is slow and the gas/vapor phase has comparatively very low viscosity. As a result, the pressure drop in the gas phase can be neglected. In cases of C_2 and higher carbon numbers, the liquid form appears to be miscible with heavy oil, and $\varphi_o = 1$. Condensable vapors are introduced at saturation pressure, and in the face of small pressure drop, $\varphi_o < 1$. All dissolved gases appear to have liquid-like specific volumes (Prausnitz et al. 1999; Mohan et al. 2017a).

Various transport aspects were considered by Butler and Mokrys (1989). The conservation-of-species equation is given by

$$\frac{\partial \varphi}{\partial t} + \frac{\partial V_p \varphi}{\partial \eta} + \frac{\partial V_n \varphi}{\partial \xi} = \frac{\partial}{\partial \eta} D \frac{\partial \varphi}{\partial \eta} + \frac{\partial}{\partial \xi} D \frac{\partial \varphi}{\partial \xi}, \quad (1)$$

where ξ and η are coordinates in the tangential and normal directions and V_p and V_n are velocities in those directions, respectively, as shown in Fig. 1. They chose as a solution

$$U\varphi = -D \frac{\mathrm{d}\varphi}{\mathrm{d}\xi}, \quad (2)$$

Original SPE manuscript received for review 14 February 2017. Revised manuscript received for review 16 August 2018. Paper (SPE 194212) peer approved 28 September 2018.

where U is the interfacial velocity. As discussed in Appendix A, we find that such an assumption does not satisfy the conservation equation (Eq. 1). After a consistent set of approximations shown in Appendix A, we obtain

$$\frac{\partial}{\partial\eta}\left(\frac{V_z\times\sin\theta}{\phi}\varphi\right)=\frac{\partial}{\partial\xi}\left(D\frac{\partial\varphi}{\partial\xi}\right), \quad \ldots\ldots (3)$$

where the downward (z) velocity is given by Darcy's law as

$$V_z=\frac{k\Delta\rho g}{\mu}, \quad \ldots\ldots (4)$$

and $V_p=V_z\times\sin\theta$. Further, $\Delta\rho$ is the difference between the local density and the density of the solvent, and is hence zero in the solvent phase; g is the acceleration due to gravity; and μ is the local viscosity. In the oil phase not yet penetrated by the solvent, the viscosity μ will be very high, and hence V_z is practically zero there. Thus, most of the flow is in the narrow interfacial region shown as a ribbon in Fig. 1, where, combining Eqs. 3 and 4,

$$\frac{\partial}{\partial\eta}\left(\frac{k\Delta\rho g\times\sin\theta}{\phi\mu}\varphi\right)=\frac{\partial}{\partial\xi}\left(D\frac{\partial\varphi}{\partial\xi}\right) \quad \ldots\ldots (5)$$

is obtained. Because Darcy's law gives us the superficial velocity and the interstitial velocity is needed in Eq. 3, the porosity ϕ has been added. At this point, the slender-body approximation (Batchelor 1967), is invoked where the shape of the interface (here, $\sin\theta$) changes only slowly with η. Assuming further that μ is a constant in the ribbon and infinite outside, and D is constant inside the ribbon and zero outside, one has

$$\frac{k\Delta\rho g\sin\theta}{\phi\mu D}\frac{\partial}{\partial\eta}\varphi=\frac{\partial^2\varphi}{\partial\xi^2} \quad \ldots\ldots (6)$$

in the ribbon. Eq. 6 has a solution (Bird et al. 2002),

$$\varphi=\varphi_o\mathrm{erfc}\frac{\xi}{\sqrt{4\mu D\eta\phi/k\Delta\rho g\sin\theta}}, \quad \ldots\ldots (7)$$

where erfc is the complementary error function. It is now possible to determine several quantities following Butler and Mokrys (1989). The thickness of the ribbon δ is given by

$$\varphi_{\min}=\varphi_o\mathrm{erfc}\frac{\delta}{\sqrt{4\mu D\eta\phi/k\Delta\rho g\sin\theta}}=\varphi_o\mathrm{erfc}(u), \quad \ldots\ldots (8)$$

where $\varphi_{\min}$ is the solvent-volume fraction on the edge of the ribbon and is defined as $\varphi_{\min}/\varphi_o=0.01$. The assumption is similar to that used by Butler and Mokrys (1989), although not identical. The variable u is defined in Eq. 8 and leads to $u=1.8225$ and $\delta\approx 1.8225\sqrt{4\mu D\eta\phi/k\Delta\rho g\sin\theta}$. The flow rate of oil collected at the bottom is

$$Q_b'=\phi\int_0^{\delta}V_p(1-\varphi)\mathrm{d}\xi|_{z=h}, \quad \ldots\ldots (9)$$

where Q_b' is the flow rate in the ribbon tangential to the interface. We have taken into account the fact that that the velocity in the production well is the superficial velocity. Substituting for φ from Eq. 7 and integrating after changing the variable from ξ to the argument on the right-hand side of Eq. 7 and integrating, one has

$$Q_b'=2\times\sin\theta\sqrt{\frac{k\phi\Delta\rho gDh}{\mu}}\left\{(1-\varphi_o)u+\varphi_o\left[u\times\mathrm{erf}(u)+\frac{(e^{-u^2}-1)}{\sqrt{\pi}}\right]\right\}. \quad \ldots\ldots (10)$$

The assumption has been made that $\eta=N=\sin\theta\times h$ at the bottom. To obtain the normal component (z-component), which is the flow rate out of the bottom of the box in Fig. 1, the right-hand side is divided by $\sin\theta$ to obtain

$$Q_b=2\sqrt{\frac{k\phi\Delta\rho gDh}{\mu}}\left\{(1-\varphi_o)u+\varphi_o\left[u\times\mathrm{erf}(u)+\frac{(e^{-u^2}-1)}{\sqrt{\pi}}\right]\right\}, \quad \ldots\ldots (11)$$

where h is the pay-zone height of the system shown in Fig. 1. The quantity within the braces is only a dimensionless number. All approximations involving $\sin\theta$ become exact if it is a constant and the interface is a straight line in Fig. 1. This is often the case, as seen in Appendix C. The solvent lost is

$$q_b=2\varphi_o\sqrt{\frac{k\phi\Delta\rho gDh}{\mu}}\left\{u-\left[u\times\mathrm{erf}(u)+\frac{(e^{-u^2}-1)}{\sqrt{\pi}}\right]\right\}, \quad \ldots\ldots (12)$$

which decreases as the solubility decreases. To derive Eq. 12, the term (1–φ) in Eq. 9 was replaced with φ. The exit-volume fraction φ_e is given by $q_b/(Q_b+q_b)$, or

$$\varphi_e=\varphi_o\left\{u-\left[u\times\mathrm{erf}(u)+\frac{(e^{-u^2}-1)}{\sqrt{\pi}}\right]\right\}\Big/u. \quad \ldots\ldots (13)$$

Because $u=1.8225$, it leads to $\varphi_e/\varphi_o=0.3084$, which reflects that the oil in solvent is leaner than the saturation concentration.

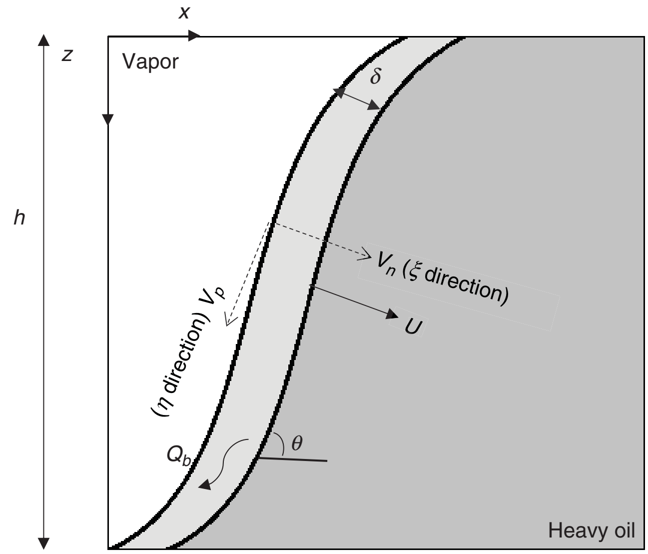

Fig. 1—Cross-sectional view of the VAPEX process, showing the region of vapor/heavy-oil interaction, adapted from Butler and Mokrys (1989). V_p and V_n are the velocities in η (tangential direction) and ξ (normal direction); h is the pay-zone height; δ is the thickness of the oil penetrated by the solvent; and U is the velocity of the interface in the direction perpendicular to the interface.

Surprisingly, the velocity of the interface U, which is very important in Butler and Mokrys (1989), has not yet made its appearance. It will appear later and will be used to determine the changes in the shapes of the interface. Since the initial submission of this manuscript, Wang et al. (2017) have provided a solution that includes the unsteady-state term and the diffusion term. The resulting solution is used to calculate the convective term, which is the oil recovered. The formulation of Wang et al. (2017) suggests that convection/oil recovered is very low and oil penetration by diffusion is high, neither of which is justified.

Concentration-Dependent Transport

The transport and thermodynamic properties are very sensitive to solvent concentrations. Previously, we have referred to D as a diffusion coefficient, when it should have been the dispersion coefficient. However, Lake (1989) has shown that the dispersion coefficient becomes the same as the diffusion coefficient at low velocities encountered in oil recovery. Consequently, for us, D is the molecular diffusivity. Further, in heavy oil, the empty space between molecules (that is, free volume) is very restricted. When the availability of free volume controls molecular movement, transport coefficients shift from the Arrhenius-activation type to the free-volume type (Cohen and Turnbull 1959; Fujita 1961; Vrentas and Duda 1979), which simplify to

$$D = D_o e^{\alpha\varphi}, \quad (14)$$

and

$$\mu = \mu_o e^{-\alpha\varphi}, \quad (15)$$

where $\alpha = B_d(e - f)/f^2$ and B_d is a constant; e and f are the free volumes of solvent and oil. Tran et al. (2012) and Mohan et al. (2017b) used the free-volume theory to satisfactorily express the transport properties of solvents in heavy crude. The diffusivity D and viscosity μ here have an inverse relationship, which is also observed in the Stokes-Einstein equation. In general, Eqs. 14 and 15 work well in the regions of low solvent concentration, where the diffusivities are very low. As a result, they describe the movement of the solvent front into the oil phase well because the low diffusivities are rate controlling. On the other hand, they do not work as well at large solvent concentrations, but that region is not involved in the rate-controlling step.

The state of a gas dissolved in oil is referred to as a condensed phase. Its implications have been discussed previously in the Introduction section. It has also been observed for three different heavy oils, that, at least for the type of solvents considered here, the volumes are additive (Tran et al. 2012; Mohan et al. 2017a, 2017b); that is, $\Delta\rho = (1 - \varphi) \times \rho_o + \varphi\rho_{sL} - \rho_{sV}$, where ρ_o is the density of pure oil, ρ_{sL} is the density of pure solvent dissolved in oil ("condensed phase"), and ρ_{sV} is the density of pure solvent in vapor form (as introduced). The relation can be rewritten as $\Delta\rho \approx \rho_o$ and $\rho_o \gg \rho_{sV}$.

Formulation. On using these results, Eq. 3 becomes

$$\frac{\partial}{\partial\eta}\left(\frac{k\rho_o g e^{\alpha\varphi} \times \sin\theta}{\phi\mu_o}\varphi\right) = \frac{\partial}{\partial\xi}\left(D_o e^{\alpha\varphi}\frac{\partial\varphi}{\partial\xi}\right). \quad (16)$$

The term $\sin\theta$ can be taken to be a constant in the neighborhood. Using this information, Eq. 16 becomes

$$\frac{k\rho_o g\sin\theta}{\phi D_o\mu_o}\frac{\partial}{\partial\eta}(e^{\alpha\varphi}\varphi) = \frac{\partial}{\partial\xi}\left(e^{\alpha\varphi}\frac{\partial\varphi}{\partial\xi}\right), \quad (17)$$

which differs from Eq. 6 by the exponential terms. Eq. 8 is solved by similarity transform (Bird et al. 2002) using the variable $s = \frac{\xi}{\sqrt{4\phi\mu_o D_o\eta/k\rho_o g\sin\theta}}$, which results in

$$-2s\frac{\mathrm{d}}{\mathrm{d}s}(e^{\alpha\varphi}\varphi)=\frac{\mathrm{d}}{\mathrm{d}s}\left(e^{\alpha\varphi}\frac{\mathrm{d}\varphi}{\mathrm{d}s}\right). \quad \ldots\ldots (18)$$

When we differentiate both sides of Eq. 18, we obtain

$$\frac{\mathrm{d}^2\varphi}{\mathrm{d}s^2}=-\alpha\left[\left(\frac{\mathrm{d}\varphi}{\mathrm{d}s}\right)^2+2s\varphi\frac{\mathrm{d}\varphi}{\mathrm{d}s}\right]-2s\frac{\mathrm{d}\varphi}{\mathrm{d}s}. \quad \ldots\ldots (19)$$

Eq. 19 is subject to the boundary conditions that $\varphi=\varphi_o$ at $s=0$ and $\varphi\to 0$ as $s\to 0$. One assumption in the formulation that follows Butler and Mokrys (1989) is that the interface is sharp. Another assumption, given in Appendix A, is that $\frac{V_p}{N}\gg\frac{V_n}{\delta}$, which will be justified after the solution is obtained (see Results and Discussion). There is also an assumption regarding the use of Darcy's law, which is discussed further in Appendix B. The numerical solutions were obtained using finite differences (central difference) **(Fig. 2)** for $\alpha\varphi_o=0$ (concentration-independent diffusivity), $\alpha\varphi_o=\infty$, and $\alpha\varphi_o=10$. The first two cases have analytical solutions of

$$\varphi=\varphi_o\mathrm{erfc}(s),\ \text{for}\ \alpha\varphi_o=0, \quad \ldots\ldots (20)$$

$$\varphi=\varphi_o\exp(-s^2),\ \text{for}\ \alpha\varphi_o=\infty. \quad \ldots\ldots (21)$$

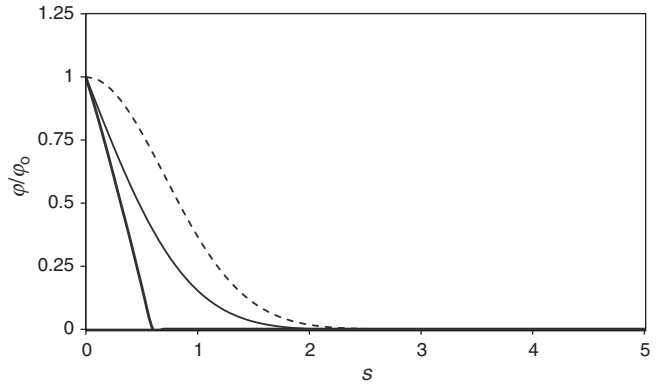

Fig. 2—Numerical solution for Eq. 19 using the central finite-difference method for $\alpha\varphi_o=0$ (thin line), $\alpha\varphi_o=\infty$ (dashed line), and $\alpha\varphi_o=10$ (thick line).

It is now possible to obtain the boundary-layer thickness from

$$\delta=\int_{\varphi_o}^{0}\xi\mathrm{d}\varphi\Big/\int_{\varphi_o}^{0}\mathrm{d}\varphi, \quad \ldots\ldots (22)$$

or in dimensionless quantities,

$$u=\int_0^1 s\mathrm{d}\psi, \quad \ldots\ldots (23)$$

which was obtained numerically. Here, $\psi=\varphi/\varphi_o$. It leads to 0.886 for $\alpha\varphi_o=\infty$, 0.3075 for $\alpha\varphi_o=10$, and 0.565 for $\alpha\varphi_o=0$ (that is, there is not much range in the values of u).

One important feature in the profiles is that except for the unrealistic case of $\alpha\varphi_o=\infty$, the other two cases of $\alpha\varphi_o=10$ and $\alpha\varphi_o=0$ show identical profiles near $s=0$. This feature will be used later.

Effect on Exit Concentrations. After the developments of Eqs. 9 through 12, we have

$$Q_b=2\sqrt{\frac{k\phi\Delta\rho gD_oh}{\mu_o}}\int_0^u e^{\alpha\varphi_o\psi}(1-\varphi_o\psi)\mathrm{d}\psi, \quad \ldots\ldots (24)$$

and

$$q_b=2\varphi_o\sqrt{\frac{k\phi\Delta\rho gD_oh}{\mu_o}}\int_0^u e^{\alpha\varphi_o\psi}\times\psi\mathrm{d}s, \quad \ldots\ldots (25)$$

where Q_b is the volume of oil/[time $\times$ width (in m)]. The integrals in Eqs. 24 and 25 are dimensionless oil recovered, $I_1=\int_0^u e^{\alpha\varphi_o\psi}(1-\varphi_o\psi)\mathrm{d}\psi$, and dimensionless solvent recovered, $I_2=\int_0^u e^{\alpha\varphi_o\psi}\times\psi\mathrm{d}s$. Both I_1 and I_2 are dependent on φ_o. Finally, the exit

concentrations are calculated. These are shown in **Table 1.** The term under the square-root sign in Eq. 24 remains the same as the results of Butler and Mokrys (1989), but the additional factors differ. We emphasize again that their assumed concentration profile does not satisfy the conservation equation for the solvent, whereas we have justified ours; both are explained in Appendix A.

	$\alpha\varphi_o = 0$	$\alpha\varphi_o = 3$	$\alpha\varphi_o = 10$	$\alpha\varphi_o = \infty$
u	0.565	0.408	0.307	–
I_1	$0.565–0.394\varphi_o$	$9.6264–4.0298\varphi_o$	$1{,}718.508–1{,}598.228\varphi_o$	–
I_2	$0.394\varphi_o$	$4.0298\varphi_o$	$1{,}598.228\varphi_o$	–
φ_e/φ_o	0.69	0.41	0.93	–

Table 1—Exit concentration calculated using the numerical solutions of Eqs. 24 and 25.

Comparison With Experiments. Butler and Mokrys (1989) showed by use of Hele-Shaw cells that the flow rate varied with the square roots of k and h. There have been a number of experimental observations since Butler and Mokrys (1989), and one significant effort to correlate the results is in the form

$$W_b = 43550(k\phi/\mu_o)^{0.51}, \quad (26)$$

by Nenninger and Dunn (2008), where W_b is the mass oil/[time × area (in m^2) through which the solvent enters the system]. Our results do have those items, with a power of 0.5. However, Eq. 26 does not have a dependence on $\sqrt{h}$. Many investigators (Karmakar and Maini 2003; Yazdani and Maini 2005; Haghighat and Maini 2012b) show a proportionality to h and not $\sqrt{h}$. Simulations by Cuthiell and Edmunds (2012) also show an h dependence. Nenninger and Dunn (2008) obtain no h dependence in the first approximation, Eq. 26. It should not be construed that there is no dependence because there is one, but scatter is very large, and W_b increases with increasing $\phi k/h^2$. It is noteworthy that they include another and newer set of data by Butler and Mokrys (1991).

As a result, we have taken a second look at the analysis, and begin by noting that Butler and Mokrys (1989) start with the Brinkman (1947) equation for velocity,

$$\frac{\mathrm{d}}{\mathrm{d}\xi}\left(\mu\frac{\mathrm{d}V_p}{\mathrm{d}\xi}\right) - \frac{\mu V_p}{k} + \Delta\rho g\sin\theta = 0, \quad (27)$$

but later ignore the first term for being small. If we assume that it is not small, then Eq. 27 needs to be solved simultaneously with Eq. 16. This must be done numerically. If we use the ribbon model here, in that the flow takes place only from $\xi = 0$ to δ, μ is a constant. We then approximate the solution to Eq. 27 as

$$V_p = a(\delta - \xi)^n, \quad (28)$$

where if $n = 0$, $V_p = a = \dfrac{k\Delta\rho g\sin\theta}{\mu}$, as before. Thus, if n is small, the velocity profile is approximately a constant given by Darcy's law, and leads to $\sqrt{h}$ dependence. If n is large, the velocity drops from Darcy's law at the interface and goes quickly to zero. The rest of the simplified calculations are given in Appendix B, which lead to $Q_b' \propto h^{\left(\frac{1+n}{2+n}\right)}$. Thus, large values of n lead to an h dependence. In Eq. 28, n is the dimensionless slope of the velocity profile at the interface. The two velocity profiles are shown schematically in **Fig. 3.**

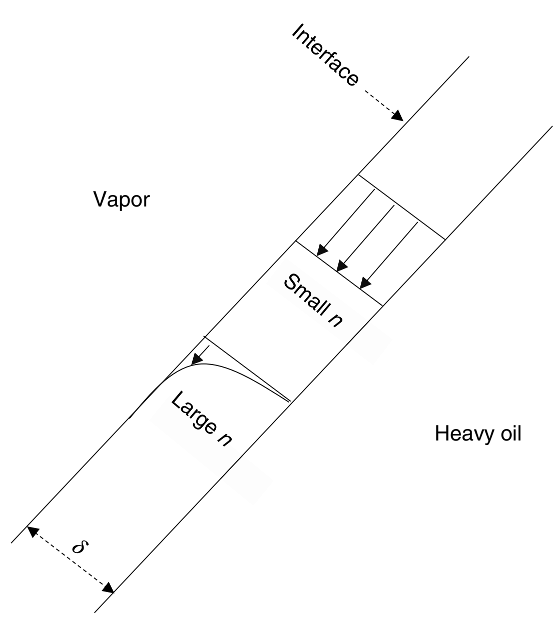

Fig. 3—Proposed velocity profiles in the model generated from Eq. 28, which for small n leads to $\sqrt{h}$ dependence and for large n to h dependence. δ is the thickness of the ribbon in the model, and there is no flow in the region occupied by the unsolvated heavy oil.

Nenninger and Dunn (2008) also noted the absence of any correlation with the physical properties of the solvent. All the solvents analyzed were at less than their critical temperatures, and the liquid form would be expected to be miscible with oil (that is, $\varphi_o = 1$ for all). One exception is CO_2, which is not miscible with heavy oil (Chung et al. 1988), and lower pressures were used by Nenninger and Dunn (2008) for the CO_2 data. Thus, φ_o is much smaller than 1.0. The CO_2 molecule is the smallest in size, and other solvents (ethane, propane, butane) do not vary much in size. Therefore, the solvent effect should have appeared for CO_2 but did not. This feature remains unexplained, although it should be noted that CO_2 provides three data points in the set of 57.

One other feature can be obtained by nondimensionalizing (or scaling) Eq. 27 for constant μ to obtain

$$\varepsilon^2 \frac{d^2 \overline{V}_p}{d\overline{\xi}^2} - \overline{V}_p + 1 = 0, \quad (29)$$

where $\overline{V}_p = V_p / (k \Delta\rho g \sin\theta / \mu)$, $\varepsilon^2 = k/L^2$, $\overline{\xi} = \xi / L$, and L is a representative macroscale. Note that both independent and dependent variables take on the order of unity. For small values of ε, the first term can be ignored, leading to Darcy's law and proportionality to $\sqrt{h}$. For values of ε that cannot be neglected, Eq. 27 needs to be solved. In addition, k itself varies by three orders of magnitude in the compilation by Nenninger and Dunn (2008). L can be taken to be h, and h varies by less than one order of magnitude in this compilation. In contrast, Eq. 29 has a simple solution and we cannot proceed with it any further, but we can with the approximate Eq. 28, as discussed in Appendix B. By equating the slope of this solution at the interface to that from Eq. 28, we obtain $n = 1/[\varepsilon \times \sinh(1/\varepsilon)]$, where as $\varepsilon = \sqrt{k/h}$ goes to zero, n goes to zero as well. Therefore, for small values of k/h^2, n will be zero, Darcy's law will hold, and $\sqrt{h}$ dependence will result; for larger values of k/h^2, an h dependence will result. The required high values of k/h^2 for this change to show are too high, probably because of the use of the approximate velocity profile. There is no hard transition, with the power of h changing from ½ to 1 continuously with increasing values of k/h^2 (or n).

Vapor/Oil Interface

The remaining issue deals with locating the oil/gas interface. Consider a point given as P^*, which is the origin of the $\eta - \xi$ coordinate shown in **Fig. 4.** Fig. 4 is mapped by the x–z system, and P^* is given by x^*, z^*.

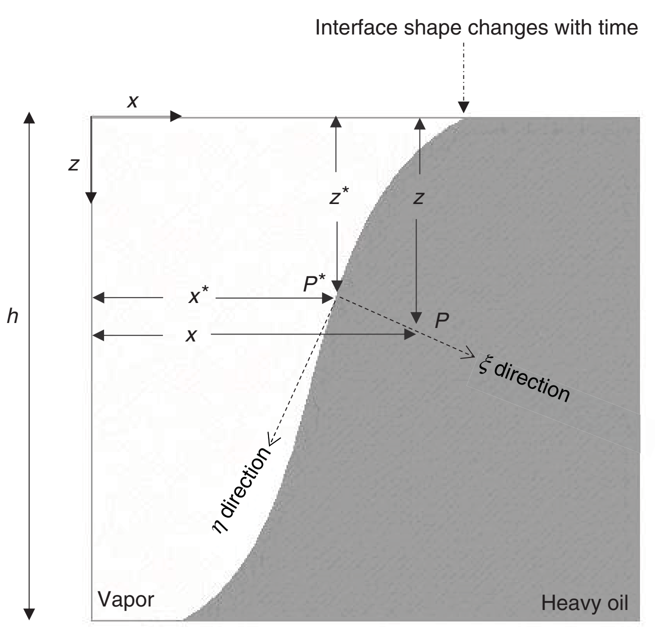

Fig. 4—Relation between the two coordinates *x–z* and *η – ξ*. The *x–z* coordinate has its origin in the top-left corner. *h* is the pay-height zone, and recovery takes place at the bottom-left corner.

The two jump balances caused by mass transfer at the interface are

$$\dot{m} = c(V_n - U) - D_o e^{\alpha\varphi_o} \frac{\partial c}{\partial \xi}, \quad (30)$$

where $\dot{m}$ is the rate of mass of the solvent transferred from the gas phase into the liquid phase, and c is the solvent concentration in the liquid. The total mass transferred is

$$\dot{m} = \rho(V_n - U), \quad (31)$$

where $\rho = (1 - \varphi)\rho_o + \varphi\rho_{sL}$ and U is the velocity at the interface in a direction normal to the interface. Note that the interfacial velocity appears only in the boundary conditions. It is being assumed here that only the solvent can move from one phase to another, and the oil cannot. Eliminating $\dot{m}$ between the two, replacing physical properties by their values at the interface, and multiplying the whole equation with $v_L = 1/\rho_{sL}$, the constant mass density of the solvent in the liquid phase, one obtains

$$v_L \rho_o (1 - \varphi_o)(V_n - U) = -D_o e^{\alpha\varphi_o} \left. \frac{\partial \varphi}{\partial \xi} \right|_{\text{interface}}. \quad (32)$$

Upon differentiation, this leads to

$$U = V_z^* \cos\theta - \frac{D_o e^{\alpha\varphi_o} \sin\theta}{v_L(1-\varphi_o)} \sqrt{\frac{kg}{\pi\rho_o\phi\mu_o D_o z^*}}, \quad (33)$$

where the superscript * symbol has been added to V_z to indicate that the physical properties used to calculate this quantity are all evaluated at the interface at solvent concentration $\varphi^* = \varphi_o$. Further, $\mu^* = \mu_o \times e^{\alpha\varphi_o}$ and η has been approximated as $z^*/\sin\theta$; η is the length of the arc representing the oil/gas interface starting from the top-right corner in Fig. 4. Thus Eq. 4 becomes

$$V_z^* = \frac{k\Delta\rho^* g}{\mu^*}, \quad (34)$$

and

$$U = \frac{\partial z^*/\partial t}{\sqrt{1+(\partial z^*/\partial x)^2}}, \quad (35)$$

(Higgins et al. 1977) where the equation of the interface is given by $z = z^*(x,t)$ and $\partial_z^*/\partial x = -\tan\theta$. It is possible to observe that at $z^* = 0$ (top-right corner in Fig. 4), the second term on the right in Eq. 33 becomes infinite. This is the legacy of the fact that there is an entrance effect, as demonstrated by the governing equation (Eq. 16), which was derived by assuming fully developed flow. The rest of the calculations are shown in Appendix C, and the approximate profiles are shown in dimensionless form in **Fig. 5.** The characteristic times and length scales used to obtain the dimensionless variables are convenient, very small, and not unique. If larger multiples of these are chosen to be in a useful range, then the shapes of the interfaces will look more linear, as discussed in Appendix C.

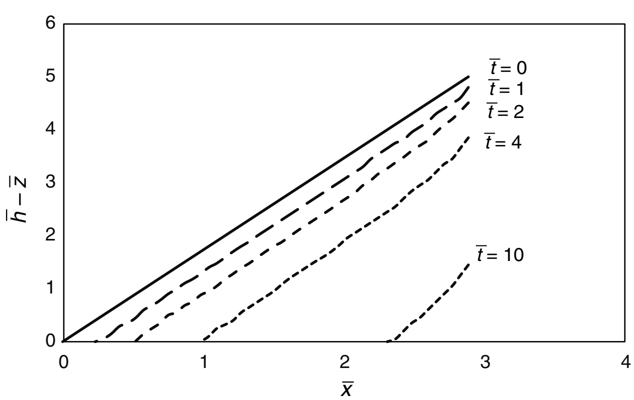

Fig. 5—Shapes of the moving oil/vapor interface shown as a function of time. All quantities are dimensionless (Appendix C), and all profiles are linear to good approximation. The slopes become steeper with increasing time. It is necessary to start with higher values of $\bar{h}$ to obtain higher values of $\bar{t}$.

Results and Discussion

We have analyzed the basic conservation equations for solvent in oil and their solutions to determine the gravity drainage of the solvated heavy oil. Butler and Mokrys (1989) start with a reasonable but assumed concentration profile; our analysis shows that this form is unsuitable. The one that is suitable gives us a governing equation that is similar to the boundary-layer equation, but provides a result for the oil recovered that is very similar to the final result of Butler and Mokrys (1989). The condition $\frac{V_p}{N} \gg \frac{V_n}{\delta}$ for the present solution can now be determined as $\frac{\delta}{N} \gg \frac{\cos\theta}{\sin\theta}$ using $V_p = \sin\theta \times V_z$ and $V_n = \cos\theta \times V_z$, the two components of Darcy's law. Further simplification can be made with $h \approx N/\sin\theta$ to obtain $\frac{\delta}{h} \gg \frac{\cos\theta}{\sin^2\theta}$. At small times, θ starts from approximately 90°, and the inequality is satisfied [see the dynamics of the Hele-Shaw cell in Butler and Mokrys (1989)]. At large times, the boundary-layer thickness increases and the inequality would also be satisfied. Thus, the basic assumption remains valid.

At the small velocities seen in oil recovery, the dispersion coefficient is the same as the diffusion coefficient. We have taken into account that the diffusivity and viscosity of solvated heavy oil are strongly dependent on solvent concentrations. The concentration profile for $\alpha\varphi_o = 10$ differs from that of $\alpha\varphi_o = 0$ (the case of no concentration dependence) in Fig. 2 because solvent penetrates into oil much less when concentration dependence is introduced (Tran et al. 2012; Mohan et al. 2017b). The case of $\alpha\varphi_o = \infty$ is of interest only because it remains bounded; it has little physical meaning. The key result from including concentration dependence in diffusivity is the reduction in solvent penetration (lower value of u). The flow rate of oil increases enormously (Table 1). This occurs because the viscosity is greatly reduced, as a result of the exponential term in Eq. 24.

We have also calculated the solvent concentration in the exit stream. We find it to be large in Table 1 for concentration-dependent transport properties. This happens because the solvent-concentration profile for $\alpha\varphi_o = 10$ in Fig. 2 is of a type where the oil can be sliced into two parts: one part is a nearly saturated slice (of thickness u), and the other part is dry. Only the nearly saturated slice will move under gravity, and the dry region will not move because of its high viscosity. Consequently, it is not surprising that the exit oil is nearly saturated. Thus, if the solvent is fully soluble (that is, $\varphi_o = 1$), then the oil that is recovered is mostly the solvent. There is a scope for optimizing the solubility of the solvent. As noted previously, Mohan et al. (2017b) found $\alpha\varphi_o$ to be approximately 10 for hexane, heptane, and toluene in heavy oil, for which $\varphi_o = 1$. Tran et al. (2012) saw α of approximately 35 for CO_2 in oil, but the highest value of φ_o of approximately 0.35 for a gas pressure of 3,000 psi. The highest value of $\alpha\varphi_o$ was approximately 10, but can be lowered

by reducing the gas pressure. As a result, in Table 1 we have also presented calculations of $\alpha\varphi_o = 3$, for which the drainage/recovery is lower but the loss of solvent is much lower.

A great amount of data has been presented since the initial work by Butler and Mokrys (1989) and has been analyzed in the light of present results. First, we do obtain a linear dependence between the rate of oil recovered and $\sqrt{(k\phi/\mu_o)}$ of Nenninger and Dunn (2008). We observe that if we move from Darcy's law to the Brinkman (1947) equation, we can find a linear h dependence, up from the $\sqrt{h}$ dependence. A key parameter that can make this shift is a large value of k/h^2. We do predict that at lower CO_2 pressures we would see a significant solvent effect compared with lower alkanes, which are not observed so far in the data.

In real heavy-oil reservoirs, k/h^2 will be very low, and all results show that the recovery will be low for such values of k/h^2. Further, the ribbon model in Appendix B predicts a penetration-depth value that is too high because of the strong variation in the transport properties with concentration. As a result, the actual recovery will be lower and the exit concentration of the solvent will be higher. The effect of the solvent on recovery cannot be seen without varying the pressures, and such data do not exist.

The evolving shape of the interface in Fig. 5 is practically linear, and this happens because the term $\bar{z}$ dominates over the rest on the left-hand side of Eq. C-5. With time, the oil/vapor interface recedes but grows steeper. As mentioned in Appendix C, the characteristic length and time scales used are small. If more-realistic scales in the form of large multiples are chosen, then the shapes of interfaces will be more linear, as discussed in Appendix C.

Conclusions

We observe that the correct formulation for the conservation equation leads to the principal group $\sqrt{(k\phi/\mu_o)}$, which determines oil production and is also proportional to the square root of the pay-zone height h. If we relax Darcy's law and move to the Brinkman (1947) equation for the correct velocity profile, we obtain a height dependence that spans $\sqrt{h}$ to h. We see a strong dependence on solvent type. As best we can generalize, a good solvent will recover more oil but the oil will be very high in the solvent. A poorer solvent will lower both the oil recovered and its solvent content. A numerical simulation would be required to progress any further in predictions or variations.

Nomenclature

B_d = solvent segment needed for a jump during diffusion
B_μ = oil segment needed for movement in viscosity
c = solvent concentration in the liquid
D = diffusivity
D_o = diffusivity at infinite dilution
e = free volume of the solvent
f = free-volume fraction of oil
g = acceleration caused by gravity
h = total pay-zone height of the system
I_1, I_2 = integral defined after Eq. 25
k = permeability
$\dot{m}$ = solvent-mass-transfer rate
n = index showing velocity variation in Eq. 28
$P*$ = a point on the interface (see Fig. 5)
q_b = solvent loss
Q'_b = flow rate in the ribbon tangential to the interface
u = dimensionless boundary-layer thickness, defined in Eq. 13
U = velocity of the interface
v_L = specific volume of pure solvent dissolved in oil
V_p = velocity in the tangential direction
V_z^* = Darcy's-law velocity at the interface
x^* = coordinate of point $P*$
z^* = coordinate of point $P*$
α = concentration-dependence term
δ = thickness of the boundary layer
$\Delta\rho$ = density difference between the oil phase and the gas phase
$\Delta\rho^*$ = $\Delta\rho$ at the interface
η = coordinate in the tangential direction
μ = viscosity
μ^* = μ at the interface
μ_o = viscosity at infinite dilution
ξ = coordinates in the normal direction
ρ = total density
ρ_o = density of pure oil
ρ_{sL} = density of pure solvent dissolved in oil
ρ_{sV} = density of pure solvent in vapor form
ϕ = porosity
φ = volume fraction of solvent
φ_e = exit volume fraction
$\varphi_{\min}$ = solvent-volume fraction on the inner edge of the ribbon
φ_o = initial volume fraction of solvent
ψ = φ/φ_o

References

Aghbash, V. N. and Ahmadi, M. 2012. Evaluation of CO_2-EOR and Sequestration in Alaska West Sak Reservoir Using Four-Phase Simulation Model. Presented at the SPE Western Regional Meeting, Bakersfield, California. SPE-153920-MS. https://doi.org/10.2118/153920-MS.

Bachu, S. and Shaw, J. 2003. Evaluation of the CO_2 Sequestration Capacity in Alberta's Oil and Gas Reservoirs at Depletion and the Effect of Underlying Aquifers. *J Can Pet Technol* **42** (9): 51–61. PETSOC-03-09-02. https://doi.org/10.2118/03-09-02.
Banerjee, D. K. 2012. *Oil Sands, Heavy Oil & Bitumen*. Tulsa: PennWell.
Batchelor, G. K. 1967. *An Introduction to Fluid Dynamics*. Cambridge, UK: Cambridge University Press.
Bird, R. B., Stewart, W. E., and Lightfoot, E. N. 2002. *Transport Phenomena*. New York City: John Wiley & Sons.
Brinkman, H. C. 1947. On the Permeability of Media Consisting of Closely Packed Porous Particles. *Appl. Sci. Res.* **A1:** 81–86.
Burke, N. E., Hobbs, R. E., and Kshou, S. F. 1990. Measurement and Modeling of Asphaltene Precipitation. *J Pet Technol* **42** (11): 1440–1520. SPE-18273-PA. https://doi.org/10.2118/18273-PA.
Butler, R. M. and Mokrys, I. J. 1989. Solvent Analog Model of Steam-Assisted Gravity Drainage. *AOSTRA J. Res* **5** (1): 17–32.
Butler, R. M. and Mokrys, I. J. 1991. A New Process (VAPEX) for Recovering Heavy Oils Using Hot Water and Hydrocarbon Vapour. *J Can Pet Technol* **30** (1): 97–106. PETSOC-91-01-09. https://doi.org/10.2118/91-01-09.
Chung, F. T. H., Jones, R. A., and Nguyen, H. T. 1988. Measurements and Correlations of the Physical Properties of CO_2-Heavy Crude Oil Mixtures. *SPE Res Eng* **3** (3): 822–828. SPE-15080-PA. https://doi.org/10.2118/15080-PA.
Cohen, M. H. and Turnbull, D. 1959. Molecular Transport in Liquids and Glasses. *J. Chem. Phys.* **31** (5): 1164–1169. https://doi.org/10.1063/1.1730566.
Cuthiell, D. and Edmunds, N. 2012. Thoughts on Simulating the Vapex Process. Presented at the SPE Heavy Oil Conference Canada, Calgary, 12–14 June. SPE-158499-MS. https://doi.org/10.2118/158499-MS.
Fujita, H. 1961. Diffusion in Polymer-Solvent Systems. In *Fortschritte Der Hochpolymeren-Forschung*, Advances in Polymer Science series, Vol. 3, 1–47. Berlin: Springer-Verlag.
Haghighat, P. and Maini, B. B. 2012a. Role of Asphaltene Precipitation in Vapex Process. *J Can Pet Technol* **49** (3): 14–21. SPE-134244-PA. https://doi.org/10.2118/134244-PA.
Haghighat, P. and Maini, B. B. 2012b. Experimental Evaluation of Heated Vapex Process. Presented at the SPE Heavy Oil Conference Canada, Calgary, 12–14 June. SPE-157799-MS. https://doi.org/10.2118/157799-MS.
Higgins, B. G., Silliman, W. J., Brown, K. A. et al. 1977. Theory of Meniscus Shape in Film Flows. A Synthesis. *Ind. Eng. Chem. Fundamen.* **16** (4): 393–401. https://doi.org/10.1021/i160064a001.
Jia, Y., Huang, L., and Sun, L. 2017. The Mechanism and Simulation Research of "Foamy Oil" During CO_2 Flooding. Presented at the Carbon Management Technology Conference, Houston, 17–20 July. CMTC-485491-MS. https://doi.org/10.7122/485491-MS.
Karmakar, K. and Maini, B. B. 2003. Experimental Investigation of Oil Drainage Rates in the Vapex Process for Heavy Oil and Bitumen Reservoirs. Presented at the SPE Annual Technical Conference and Exhibition, Denver, 5–8 October. SPE-84199-MS. https://doi.org/10.2118/84199-MS.
Kok, M. V. and Ors, O. 2012. The Evaluation of an Immiscible-CO_2 Enhanced Oil Recovery Technique for Heavy Crude Oil Reservoirs. *Energ. Sour. A* **34** (8): 673–681. https://doi.org/10.1080/15567036.2011.601796.
Lake, L. W. 1989. *Enhanced Oil Recovery*. Upper Saddle River, New Jersey: Prentice-Hall.
Mohan, V., Neogi, P., and Bai, B. 2017a. Flory-Huggins Solution for Heavy Oils. *Can. J. Chem. Eng.* **95** (4): 796–798. https://doi.org/10.1002/cjce.22707.
Mohan, V., Neogi, P., and Bai, B. 2017b. Concentration Dependent Diffusivities of Model Solvents in Heavy Oil. *Diffusion Fundamen.* **27** (3): 1–27.
Naderi, K. and Babadagli, T. 2012. Experimental Analysis of Heavy Oil Recovery and CO_2 Storage by Alternate Injection of Steam and CO_2 in Deep Naturally Fractured Reservoir. Presented at the SPE Heavy Oil Conference Canada, Calgary, 12–14 June. SPE-146738-MS. https://doi.org/10.2118/146738-MS.
Nenninger, J. E. and Dunn, S. G. 2008. How Fast is Solvent Based Gravity Drainage? Presented at the Canadian International Petroleum Conference, Calgary, 17–19 June. PETSOC-2008-139. https://doi.org/10.2118/2008-139.
Nghiem, L. X. and Coombe, D. A. 1997. Modeling Asphaltene Precipitation During Primary Depletion. *SPE J.* **2** (2): 170–176. SPE-36106-PA. https://doi.org/10.2118/36106-PA.
Prausnitz, J. M., Lichtenthaler, R. N., and de Azevedo, E. C. 1999. *Molecular Thermodynamics of Fluid Phase Equilibrium*, third edition. Englewood Cliffs, New Jersey: Prentice-Hall.
Schlichting, H. 1968. *Boundary-Layer Theory*, sixth edition. New York City: McGraw-Hill.
Shaw, J. and Bachu, S. 2002. Screening, Evaluation, and Ranking of Oil Reservoirs Suitable for CO_2-Flood EOR and Carbon Dioxide Sequestration. *J Can Pet Technol* **41** (9): 51–61. PETSOC-02-09-05. https://doi.org/10.2118/02-09-05.
Temizel, C., Balaji, K., Suhag, A. et al. 2017. Optimization of Foamy Oil Production in Horizontal Wells. Presented at the SPE Latin America and Caribbean Mature Fields Symposium, Salvador, Bahia, Brazil, 15–16 March. SPE-184904-MS. https://doi.org/10.2118/184904-MS.
Tran, T. Q. M. D., Neogi, P., and Bai, B. 2012. Free Volume Estimates of Thermodynamic and Transport Properties. *Chem. Eng. Sci.* **80** (1 October): 100–108. https://doi.org/10.1016/j.ces.2012.06.012.
Vrentas, J. S. and Duda, J. L. 1979. Molecular Diffusion in Polymer Solutions. *AIChE J.* **25** (1): 1–24. https://doi.org/10.1002/aic.690250102.
Wang, Q., Jia, X., and Chen, Z. 2017 Modelling of Dynamic Mass Transfer in a Vapour Extraction Heavy Oil Recovery Process. *Can. J. Chem. Eng.* **95** (6): 1171–1180. https://doi.org/10.1002/cjce.22743.
Yazdani, A. and Maini, B. B. 2005. Effect of Height and Grain Size on the Production Rates in the Vapex Process: Experimental Study. *SPE Res Eval & Eng* **8** (3): 205–212. SPE-89409-PA. https://doi.org/10.2118/89409-PA.

Appendix A—Examining Approximations

If η and ξ, shown in Fig. 1, are the coordinates in directions tangential and normal to the interface, then the continuity equation can be written as

$$\frac{\partial \rho}{\partial t}+\frac{\partial \rho V_p}{\partial \eta}+\frac{\partial \rho V_n}{\partial \xi}=0, \qquad \text{(A-1)}$$

where V_p and V_n are the velocities in η (tangential direction) and ξ (normal direction). From Schlichting (1968), if the order of η is N, the total length of the interface, and of ξ is $\acute{o}$, the thickness of the interfacial region penetrated by the solvent, then it is expected that $N \gg \acute{o}$ and $V_p \gg V_n$. For constant ρ, the estimates in Eq. A-1 become $\frac{V_p}{N}+\frac{V_n}{\delta}$. If the two terms are comparable, then the boundary-layer theory holds. However, the present case is somewhat different because the two velocities are related, $V_p=\sin\theta \times V_z$ and $V_n=\cos\theta \times V_z$, where V_z is given by Darcy's law in Eq. 4 and the angle θ is shown in Fig. 1. Consequently, we examine $\frac{V_p}{N} \gg \frac{V_n}{\delta}$ or $\frac{V_p}{N} \ll \frac{V_n}{\delta}$. Both cases are considered separately here. The conservation of the solvent in the oil phase is given by Eq. 1, where the

assumption is made that in the solution the individual volumes are additive. If the process is slow, then term by term Eq. 1, on neglecting the unsteady-state term, leads to $\frac{V_P\varphi_o}{N}+\frac{V_n\varphi_o}{\delta}=D\frac{\varphi_o}{N^2}+D\frac{\varphi_o}{\delta^2}$. The first term on the right-hand side is negligible compared with the second, and hence for the first case that $\frac{V_p}{N}\gg\frac{V_n}{\delta}$, Eq. 1 becomes

$$\frac{\partial V_p\varphi}{\partial\eta}=\frac{\partial}{\partial\xi}D\frac{\partial\varphi}{\partial\xi}, \quad \text{(A-2)}$$

which is similar to the boundary-layer equation. However, if $\frac{V_p}{N}\ll\frac{V_n}{\delta}$, then

$$\frac{\partial V_n\varphi}{\partial\xi}=\frac{\partial}{\partial\xi}D\frac{\partial\varphi}{\partial\xi}, \quad \text{(A-3)}$$

which is the equation governing concentration polarization. The unsteady-state terms have been neglected in Eqs. A-2 and A-3 because the process is very slow. This is the quasistatic assumption, and it requires us to show the unsteady nature of the process in the form of the changing shape of the interface.

Consider Eq. A-3. The only independent variable is ξ, and integrating once,

$$V_n\varphi=D\frac{d\varphi}{d\xi}+C, \quad \text{(A-4)}$$

where the constant of integration is found to be zero using the boundary conditions that as $\xi\to\infty$ (interior of the oil phase), φ and $d\varphi/d\xi\to 0$. We obtain

$$V_n\varphi=D\frac{d\varphi}{d\xi}. \quad \text{(A-5)}$$

Instead of solving the equation for conservation of solvent in the oil phase, Butler and Mokrys (1989) assume a solution in the form given by Eq. 2. Adding Eqs. A-5 and Eq. 2, we obtain $U=-V_n$ or $\varphi=0$ at the interface, a result that says that the two velocities move in two different directions or that there is no dissolution. This approximation is discarded. The implication is that the approximation by Butler and Mokrys (1989), Eq. 2, does not satisfy the conservation of species.

If in Eq. A-2, V_p is replaced with the η component of V_z, the component in the downward direction and θ between η and z are shown in Fig. 1. Then Eq. 3 results, which has been adopted here.

Appendix B—Brinkman Equation for Flow

The Brinkman (1947) equation is in the present form

$$\frac{d}{d\xi}\left(\mu\frac{dV_p}{d\xi}\right)-\frac{\mu V_p}{k}+\Delta\rho g\sin\theta=0. \quad \text{(B-1)}$$

Take $V_p=a(\delta-\xi)^n$, where if $n=0$, we obtain $V_p=a=\frac{k\Delta\rho g\sin\theta}{\mu}$. Then, substituting this velocity profile into Eq. 3, we obtain

$$\frac{\partial}{\partial\eta}\left[\frac{a(\delta-\xi)^n}{\phi}\varphi\right]=\frac{\partial}{\partial\xi}\left(D\frac{\partial\varphi}{\partial\xi}\right). \quad \text{(B-2)}$$

We use the ribbon model, Eqs. 6 through 13, where $V_p=0$ at the edge of the ribbon at $\xi=\delta$, and D and μ are constants in the ribbon. Following Bird et al. (2002), the similarity variable is found to be $\chi=by/\eta^{1/(2+n)}$, where $y=\delta-\xi$, $b^{2+n}=\frac{a}{\phi D}$, and Eq. B-2 becomes

$$-\frac{1}{2+n}\chi^{1+n}\frac{d\varphi}{d\chi}=\frac{d^2\varphi}{d\chi^2}. \quad \text{(B-3)}$$

In other words, φ is a function of a single variable, χ. Eq. B-3 is to be solved subject to the boundary conditions $\varphi=\varphi_o$ at $\xi=0$ or $\chi=\frac{b\delta}{\eta^{1/(2+n)}}$, and $\varphi=0$ at $\xi=\delta$ or $\chi=0$.

The first boundary condition cannot be satisfied under similarity transform, because the interface is described by an equation of η, unless

$$\delta=c\times\eta^{1/(2+n)}. \quad \text{(B-4)}$$

That is, the boundary-layer thickness/width of the ribbon increases as we go downward. Then, the interface becomes $\chi=$constant, and a full solution for φ is possible. Substituting for the velocity V_p in Eq. 9 and rearranging, we obtain

$$Q_b'=\phi\int_0^{\delta}a(\delta-\xi)^n(1-\varphi)d\xi. \quad \text{(B-5)}$$

Moving to the similarity group, Eq. B-5 becomes

$$Q_b'=\frac{\phi\eta^{\frac{n+1}{n+2}}}{(n+1)b^{n+1}}\int_{\chi=0}^{\chi=b\delta/\eta^{1/(2+n)}}(1-\varphi)d\chi^{n+1}, \quad \text{(B-6)}$$

where the integration is performed from one end of the ribbon to the other. Because $(1–\varphi)$ is continuous and positive, it can be replaced with an average $\overline{(1-\varphi)}$, and the integral becomes

$$Q'_b = \frac{\phi a}{(n+1)}\overline{(1-\varphi)} \times \delta^{n+1}. \quad \text{(B-7)}$$

Eq. B-4 shows $\delta \propto \eta^{\frac{1}{2+n}}$, and substituting into Eq. B-6, it is seen that $Q'_b \propto \eta^{\left(\frac{1+n}{2+n}\right)}$, or, at the bottom, $Q'_b \propto N^{\left(\frac{1+n}{2+n}\right)}$ or $\propto h^{\left(\frac{1+n}{2+n}\right)}$. N is approximately $h/\sin\theta$. Note that at $n=0$, the proportionality is to $\sqrt{h}$. It is only when n is very large that we see proportionality to h. The difference between the two velocity profiles is sketched in Fig. 3.

Appendix C—Shapes of Interfaces

Combining Eqs. 33 through 35, using many small identities given there and approximating $\eta = z^*/\sin\theta$, we obtain

$$\frac{\partial z^*}{\partial t} = \frac{k\Delta\rho^* g}{\mu^*} - \frac{e^{\alpha\varphi_o}\tan\theta}{v_L(1-\varphi_o)}\sqrt{\frac{kgD_o}{\pi\rho_o\phi\mu_o z^*}}. \quad \text{(C-1)}$$

Eq. C-2 is nondimensionalized to $\overline{z} = z^*/\ell$ and $\overline{t} = t/\tau$, where

$$\ell = \frac{1}{(v_L\Delta\rho^*)^2}\frac{D_o\mu_o}{kg\phi\rho_o}\frac{1}{(1-\varphi_o)^2}, \quad \text{(C-2)}$$

$$\tau = \frac{\ell\mu_o}{k\Delta\rho^* g e^{\alpha\varphi_o}}, \quad \text{(C-3)}$$

leading to

$$\frac{\partial\overline{z}}{\partial\overline{t}} = 1 - \frac{\tan\theta}{\sqrt{\pi\overline{z}}}. \quad \text{(C-4)}$$

Eq. C-4 represents a partial-differential equation and a moving-boundary problem where $\partial\overline{z}/\partial\overline{x} = -\tan\theta$. Here, $\overline{x} = x/\ell$. It can be simplified by setting $\tan\theta$ by an average value $\langle\tan\theta\rangle$ because it does not show strong variations. In that case, Eq. C-4 can be integrated to give

$$2[\overline{z} + <\tan\theta>\sqrt{\overline{z}}/\sqrt{\pi} + <\tan\theta>^2\ln(\sqrt{\overline{z}} - <\tan\theta>/\sqrt{\pi})] = \overline{t} + f, \quad \text{(C-5)}$$

where f is a function of $\overline{x}$. The initial profile is taken to be that of a straight line at angle θ_o, or

$$(\overline{h} - \overline{z}) = \tan\theta_o \times \overline{x}, \quad \text{(C-6)}$$

where $\overline{h} = h/\ell$. Thus, at time $\overline{t} = 0$, we have $\partial\overline{z}/\partial\overline{x} = -\tan\theta_o$. To eliminate unbounded behavior in the logarithmic term in Eq. C-5, we augment $\overline{z}$ in Eq. C-5 to $\overline{z} + \overline{z}_o$, where

$$\overline{z}_o = \tan\theta_o/\sqrt{\pi}. \quad \text{(C-7)}$$

The effect of $\overline{z}_o$ as $\overline{z}$ becomes large is diminished, and for small values of $\overline{z}$ cancels at least the unphysical entrance effects.

The procedure now is to set θ_o at 60°, and the initial profile passes through $\overline{z} = \overline{h}$ and $\overline{x} = 0$. Eq. C-6 is used to eliminate $\overline{z}$ between Eqs. C-5 and C-6 at time $\overline{t} = 0$. This gives us f as a function of $\overline{x}$. $<\tan\theta>$ is taken to be unity. Next, we can go to a higher value of time, such as $\overline{t} = 1$. The right-hand side of Eq. C-5 becomes $1 + f$ and a known function of $\overline{x}$, which can be used for every value of $\overline{x}$, to calculate a value for $\overline{z}$ and $<\tan\theta> = 1$. The solutions are made more accurate by calculating and using the derivative $\partial\overline{z}/\partial\overline{x}$ from the profiles of the previous timestep. Such a solution is shown in Fig. 5 in the form of $\overline{h} - \overline{z}$ as a function of $\overline{x}$ at $\overline{t} = 1$. Realistic values of ℓ and τ are very small. However, they can be increased, such as by a factor of 10^6; the result is that the second term on the right-hand side decreases by a factor of 10^{-3}. The solutions now are more inclined toward straight lines.

Vijitha Mohan earned a PhD degree in chemical engineering from the Missouri University of Science and Technology and served as a lecturer after graduation. Her research interests lie in heavy-oil recovery. Mohan has authored or coauthored two previous publications in this area of research. She holds a bachelor's degree in chemical engineering from the University of Madras, India, and a master's degree in chemical engineering from Mississippi State University.

Parthasakha Neogi is a professor of chemical engineering at Missouri University of Science and Technology, where he has served on the faculty for the last 36 years. His research interests are in wetting, surfactants and polymers, and in interfacial transport phenomena. Neogi holds a bachelor's degree from the Indian Institute of Technology, Kharagpur; a master's degree from the Indian Institute of Technology, Kanpur; and a PhD degree from Carnegie-Mellon University, all in chemical engineering. He is a member of SPE.

Baojun Bai holds the Lester R. Birbeck Endowed Chair and is a professor of petroleum engineering at the Missouri University of Science and Technology. Previously, he was a reservoir engineer and head of the conformance-control team at the Research Institute of Petroleum Exploration and Development, PetroChina. Bai was also a post-doctoral-degree scholar at the California Institute of Technology and a graduate research assistant at the New Mexico Petroleum Recovery Research Center for enhanced-oil-recovery projects. He has more than 20 years of experience in the area of enhanced oil recovery. Bai has authored or coauthored more than 130 papers for peer-reviewed journals and international conferences. He holds PhD degrees in petroleum engineering from the New Mexico Institute of Mining and Technology and in petroleum geology from China University of Geosciences, Beijing. Bai served on the *JPT* Editorial Committee for the feature "EOR Performance and Modeling" from 2007 to 2013. He is a member of SPE and a technical editor for *SPE Journal* and *SPE Reservoir Evaluation & Engineering*.